Numerical analysis of dynamic loads in pavement structures based on the subgrade material of MSWI bottom ash

Chen Ji [i)], Yang Jianxin [ii)], Chen Yanhong [ii)], Li Bin [i)], Huang Yucheng [iii)] and Tang Qiang [iv)]

i) Master Candidate, School of Rail Transportation, Soochow University. Xiangcheng District, Suzhou 215131, China.
ii) Senior Researcher, China Railway Tenth Group of The Fifth Engineering Co., Ltd, Gaoxin District, Suzhou 215011, China.
iii) Doctoral Researcher, School of Rail Transportation, Soochow University. Xiangcheng District, Suzhou 215131, China.
iv) Professor, School of Rail Transportation, Soochow University. Xiangcheng District, Suzhou 215131, China.

ABSTRACT

With the rapid promotion of city urbanization, the amount of municipal solid waste (MSW) is increasing. Incineration can significantly reduce the mass, volume and generate energy at the meanwhile, making it a mainstream approach for recycle of MSW. The process of incineration brings about various benefits, such as good capacity reduction, high quality reduction, effective removal of harmful components, and high efficiency of resource reuse. The utilization of MSWI bottom ash can achieve the purpose of energy conservation, emission reduction and resource recycling. Recently, MSWI has been successfully recycled for many applications, especially in road construction. Many simulation studies have conducted it as substitutable material in subgrade layer, owing to the similarity to traditional mineral aggregate. It is indispensable to develop a resistance as subgrade layer, and the purpose of this paper is to investigate the feasibility of MSWI bottom ash for practical application in subgrade layer. For this reason, an ABAQUS finite element simulation model of pavement structure subjected to dynamic loads has been conducted.

Keywords: MSWI bottom ash, three-dimensional pavement model, dynamic load simulation

1 INTRODUCTION

With the increase of population and the expansion of the city scale, the amount of municipal solid waste (MSW) has been increased rapidly. In view of the protection of the environment and the reuse of resources, the disposal and recycling of MSW has been a critical worldwide concern (Tang et al., 2018a, 2019a; Shen et al., 2019; Bakker et al., 2007). The output of waste for incineration and landfill in China approaches 500 million tons a year, which accounts for 30% of the world and ranks the second across the globe just behind United States. As a result, if the disposal of MSW is neglected, the amount of MSW every year is a potential threat to the environment and human health (Tang et al., 2017; Alam et al., 2017). At present, there are many ways of MSW disposal, such as sanitary landfill, incineration, recycling, anaerobic digestion, compositing, etc., among which the first three are most used (Tang et al., 2016a; Arickx et al., 2007).

The incineration process transforms the thermal energy of the combustible part of the waste through combustion, possessing a wide variety of benefits, including good capacity reduction, high quality reduction, effective removal of harmful components, and high efficiency of resource reuse (Wang et al., 2018; Bian et al., 2018; Tang et al., 2015). Therefore, the incineration can be well combined with other waste disposal methods at the same time. In many countries, the proportion of incineration is dominant, such as Switzerland and Japan. After the incineration process, a part of ash residue is remained. The ash residue is mainly composed of two parts, while MSWI bottom ash accounts for 80% and the rest is MSWI fly ash (Vegas et al., 2008; Tang et al., 2018b; Alba et al., 1997). MSWI bottom ash mainly contains silicate, oxide and carbonate, and the elements are Si, Ca, Fe, Al, Na, K, Mg, Cl, in addition to a certain amount of Ag, B, Ba and other elements (Bayuseno et al., 2010; Zhang et al., 2019a). Generally, the bottom ash belongs to the non-toxic and harmless waste according to the current standards. In consonance with previous studies, the material composition of MSWI bottom ash is diverse and complex, with good mechanical properties, which is suitable for resource reuse (Zhang et al., 2019b; Tang et al., 2014).

In recent years, the utilization of MSWI in civil engineering has been developing rapidly. Due to the development of new and sustainable building materials, MSWI has been tested and practically applied, especially in road construction. MSWI bottom ash is now used as roadbed filling, and quite a lot of studies have been conducted to further research whether MSWI bottom ash is the appropriate and reasonable for road

construction (Zhang Y et al., 2018; Seng et al., 2020). The properties and actual performance have been researched through series of tests in our early studies (Huang et al., 2020). It is confirmed that MSWI bottom ash is suitable for application in road construction. The recycle of MSWI bottom ash in road construction can not only solve the overuse of land resources caused by landfilling, but also achieve the purpose of economical utilization and environmental protection as well as human-health (Zhang et al., 2020; Huang et al., 2017a). At the same time, MSWI layer has been conducted in many finite element simulations. It is confirmed that MSWI bottom ash is similar to traditional subgrade material, and is suitable to be set above the subgrade layer. As a part of road tests, the dynamic loading model of MSWI bottom ash in subgrade structure is indispensable (Tang et al., 2009; Huang et al., 2017b; Wen et al., 2015).

In this paper, an ABAQUS finite element dynamic loading model of pavement structure has been conducted to investigate the validity of MSWI bottom ash as subgrade materials. The objective is 1) to distinguish the effect of stress diffusion within MSWI layer, 2) to investigate the strain at the underside of the hot mix asphalt (HMA) with/without MSWI layer and the stress diffusion through the depth, 3) to verify whether the thickness change of MSWI layer affect the stress and strain significantly.

2 ABAQUS DYNAMIC LOADING MODEL

2.1 Simplified pavement model

In this paper, the three-dimensional pavement model is simulated by commercial finite element software ABAQUS. As shown in Fig. 1, the model is divided into four layers, while the length of the model is 2.6m (load moving direction) and the width is 2m. The simulated moving load wheel track area is assumed to be in the middle of pavement surface, which is 0.3m in width and 0.96m in length. These four components are set successively from the top to the bottom of the dynamic loading model.

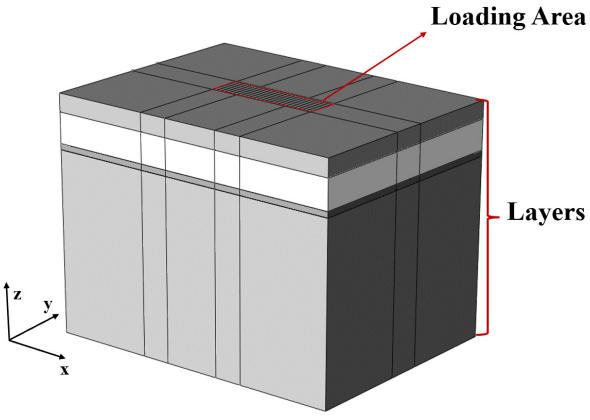

Fig. 1. Simplified pavement model.

2.2 Pavement structures and material properties

Pavement structures were developed to evaluate the features of pavement with/without MSWI layer. As illustrated in Fig. 2(a), the pavement structure without MSWI layer consists of HMA, unbound granular base, and subgrade, with the thickness of 15cm, 25cm and 1.5m. In Fig. 2(b), the structure with MSWI layer is displayed. Three pavement structures with different thickness of MSWI layer were developed. The thickness varies from 5cm to 15cm, while the total thickness of MSWI layer and subgrade layer is invariant.

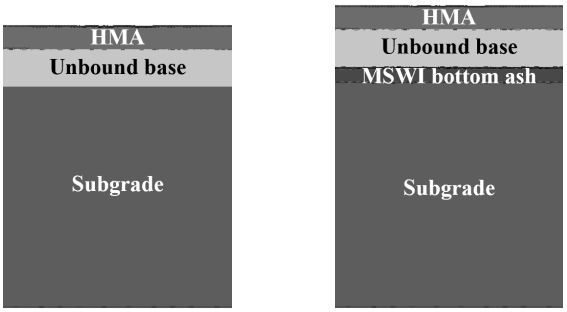

a. Without MSWI bottom ash. b. With MSWI bottom ash.

Fig. 2. Pavement structures.

The properties of the four layers are shown in Table 1. The resilient modulus is estimated from CBR values, according to the conversion described by the Asphalt Institute's Soils Manual for the Design of Asphalt Pavement Structures (Tang et al., 2016b, 2019b; Gajewski et al., 2008). The values of CBR tests have been done in previous studies. The conversions equation between CBR values and resilient modulus of MSWI is as follows:

$$\mathrm{Mr\ (Mpa)} = 10.342\mathrm{CBR} \quad (1)$$

Table 1. Material properties.

Materials	Mass Density (g/mm^3)	Young's Modulus E (Pa)	Poisson Ratio v
HMA	2700	2.1×10^9	0.35
Unbound Base	2100	0.2×10^9	0.40
MSWI	1200	1.55×10^9	0.40
Subgrade	1800	7×10^7	0.40

2.3 Surface Constraints and Boundary Conditions

In terms of model constraints, contact surface constraints and boundary constraints are mainly set in this pavement model. As shown in Fig. 3(a), the three surface constraints between HMA layer, unbound base layer, MSWI layer and subgrade layer have been marked out. These three surface constraints mainly used to simplify contact conditions and mesh generation (Hambleton et al., 2009; Luo et al., 2017; Zhang J et al., 2017). Boundary Conditions in this

model is shown in Fig. 3(b). The boundary conditions of four sides around the model are (XSYMM, U1=UR2=UR3=0) and (YSYMM, U2=UR1=UR3=0) respectively, and the boundary conditions of opposite sides are the same. It means that the layers extend infinitely along the four directions (±X and ±Y) without being affected by boundary constraints. The bottom of the model is completely fixed with boundary condition of (U1=U2=U3=UR1=UR2=UR3).

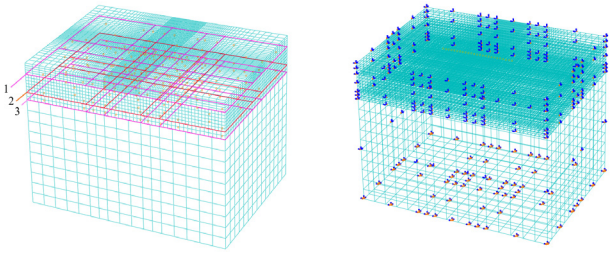

a. Surface constraints. b. Boundary conditions.

Fig. 3. Surface constraints and boundary conditions.

2.4 Moving load and steps

In order to be more accurate and closer to the reality, the shifting load pressure is utilized to simulate moving tire load. The loading area between tire and pavement is assumed to be a rectangle of 24 × 0.04 meters long and 0.3 meters wide. The loading area is divided into 6 elements, each with 0.04 meters in width. As shown in Fig. 4, the entire moving tire load track consists of 24 elements in longitudinal direction. The parameters of loading area and tire moving load are shown as follow in Table 2:

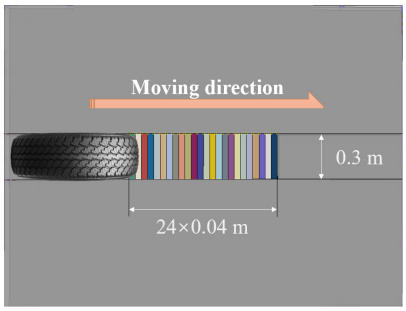

Fig. 4. Moving tire load schematic.

Table 2. Parameters of moving tire load.

Parts	Area	Moving load			
Parameters	Size/m × m	Pressure /Pa	Steps	Length /m	Speed /km/h
Value	0.96 × 0.3	690000	24	6 × 0.04	60

The loading steps of the pavement structure is shown in Fig. 5. As illustrated in Fig. 5(a), there are 24 steps of consecutive loading. At the initial step, there exists no load on the loading area and the tire is unlocked on the left of the first element. The tire load is moving along the load moving direction at a speed of 60 km/h, and the dwell time on each element is 0.0024 s. At step #1, the load is exerted on element #1, then exerting the load on element #2 when it comes to the next step. The whole moving load of tire imposed on the elements at step #6. Then the moving load is removed on element #1 and exerted on the element #7. The load is moving in this way until passes the loading area as one load cycle at step #24, as shown in Fig. 5(b).

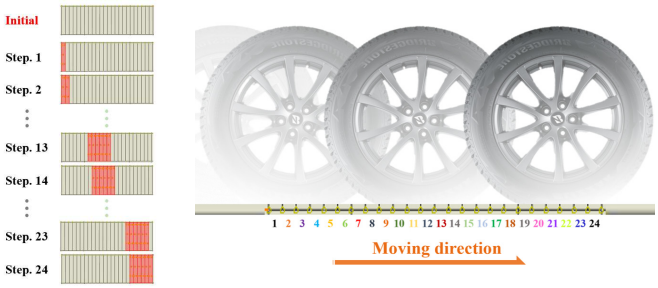

a. Loading steps. b. Loading step of moving tire load.

Fig. 5. Loading step schematic.

3 RESULTS AND DISCUSSION

3.1 Total stress and deformation (S and U)

As illustrated in Fig. 6, it is easy to distinguish the effect of total stress diffusion with/without MSWI layer. The total stress refers to the pavement model bearing stress from three vertical directions of X, Y and Z, and is often called as Mises Stress. The total stress in Fig. 6(b) is slightly lower than in Fig. 6(a), mainly because the MSWI layer weaken the diffusion of stress, and there is almost no stress change in the subgrade layer. The results show that MSWI layer plays a role of total stress diffusion on subgrade layer (Gao et al., 2019; He et al., 2020).

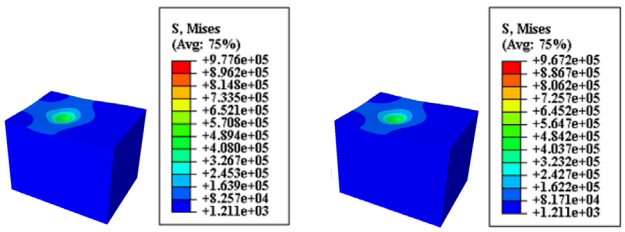

a. Without MSWI layer. b. With 5cm MSWI layer.

Fig. 6. Total stress nephogram (Mises).

The trend of the total displacement and total stress is similar. As shown in Fig. 7, the total displacement in the model with MSWI layer is a little bit lower than that without MSWI layer. The total displacement of the upper layer decreases slightly with the depth increases. To the end, there is almost no displacement change in the subgrade layer, which is the same as the trend of stress (Hossam et al., 2019).

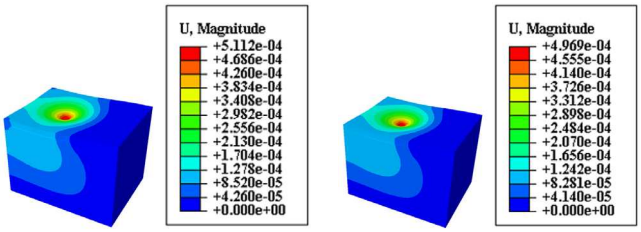

a. Without MSWI layer. b. With 5cm layer.

Fig. 7. Total displacement nephogram (Magnitude).

3.2 Stress and deformation of MSWI bottom ash

Figure 8 explained the total stress variation concerning the thickness change (0cm, 5cm, 10cm, 15cm) of MSWI layer. The total stress decreases with the thickness of MSWI increases from 0cm to 15cm, and the falling rate increases when the thickness is 0cm to 10cm. But the total stress between 10cm and 15cm decreases slower than 0cm to 10cm, which means that excessive thickness doesn't account for better performance. Moreover, when the thickness increases, the subgrade layer bear more stress. The stress in the subgrade layer decreases slightly when the thickness is 10 cm, while it increases obviously when the thickness reaches 15cm. This phenomenon may be caused by the complicated diffusion of the stress due to the excessive thickness (Aaron et al., 2013).

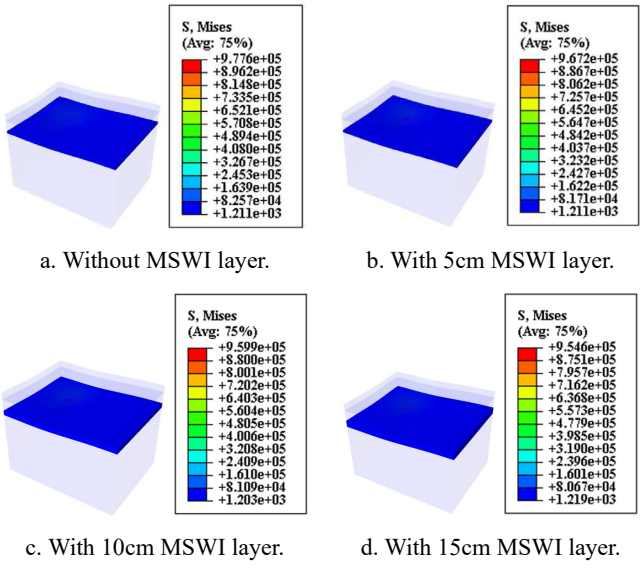

a. Without MSWI layer. b. With 5cm MSWI layer.

c. With 10cm MSWI layer. d. With 15cm MSWI layer.

Fig. 8. Stress nephogram (Mises) of MSWI layer.

Figure 9 depicts the deformation top of MSWI layer with different layer thickness when subjected to moving tire load. With the thickness increases, the displacement decreases while magnitude is smaller, which is not hard to understand through the above stress changes. It can be concluded that a certain extent of thickness plays an important role in stress diffusion. However, when the thickness increases to a certain figure, the rigidity of this layer is large, resulting in an unsatisfactory stress distribution (Dae-Wook., 2007).

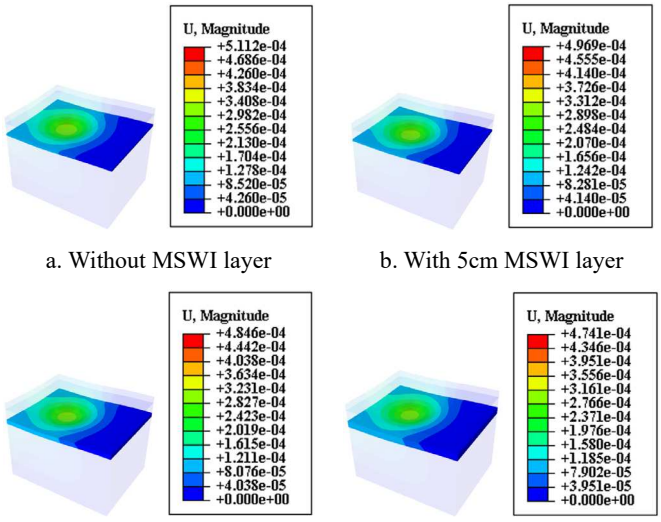

a. Without MSWI layer b. With 5cm MSWI layer

c. With 10cm MSWI layer. d. With 15cm MSWI layer.

Fig. 9. Deformation nephogram (Magnitude) of MSWI layer.

3.3 Stress and deformation of MSWI bottom ash

The longitudinal and transverse strain history at the underside of the HMA layer with/without MSWI layer is shown in Fig. 10. Strain history from two vertical directions (X-S11, Y-S22) are depicted, and the trend is similar.

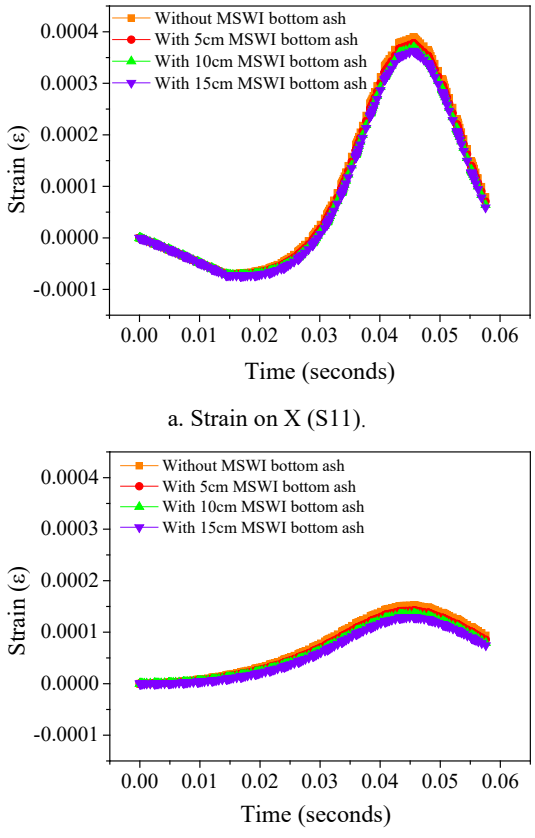

a. Strain on X (S11).

b. Strain on Y (S22).

Fig. 10. Strain at underside of HMA layer.

The presence of MSWI layer decreases the strain at underside of HMA layer, which is more pronounced at peak. With the increase of thickness, the stress decreases gradually, and the trend on X and Y is the same. However, when the thickness increases to 15cm, the change of strain decreases. It can be concluded that adding a MSWI layer on the subgrade layer diminishes the strain at the bottom of HMA layer (Peng et al., 2020).

3.4 Vertical compressive stress and strain through depth

Figure 11 explained the stress diffusion through the depth of the pavement model. The presence of MSWI bottom ash slightly decreases the compressive stress through the depth of pavement, the values are analogous in the four models.

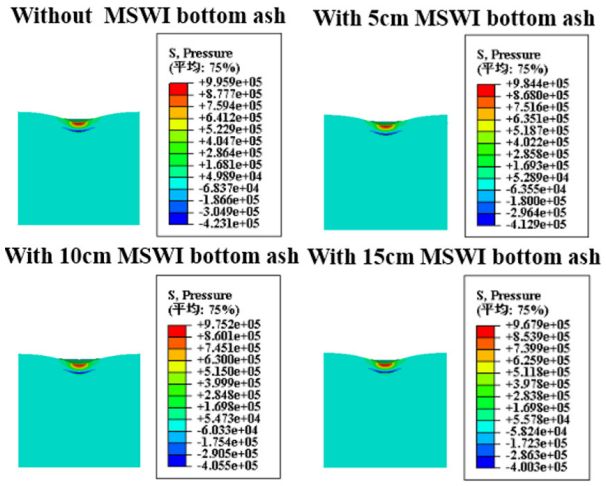

Fig. 11. Vertical compressive stress through depth.

With the thickness of MSWI layer increases, the stress decreases gradually, and the magnitude decreases when the thickness reaches to 15cm. As shown in Fig. 12, the trend is similar to the changing mode of compressive stress.

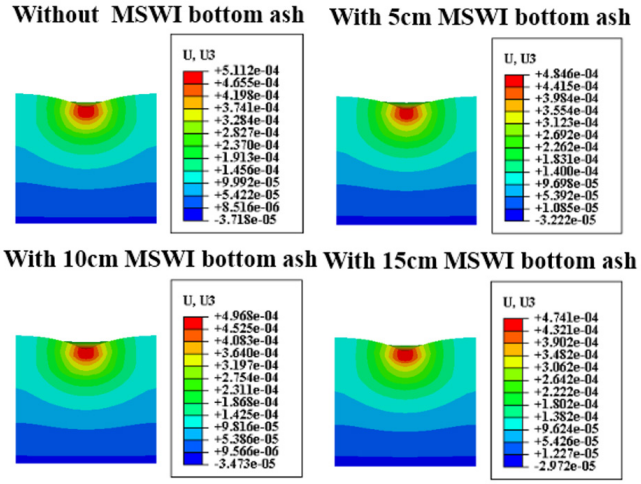

Fig. 12. Vertical compressive strain through depth.

To be concluded, a MSWI bottom ash layer on the subgrade layer lessens the compressive strain on top of subgrade layer. It is confirmed that the MSWI layer alleviate the fatigue and damage due to dynamic loads (Salehabadi et al., 2012; Reaz et al., 2016).

4 CONCLUSIONS

In this paper, an ABAQUS finite element dynamic tire loading model of pavement structure has been conducted to investigate the validity of MSWI bottom ash as subgrade materials. By developing this model, it is intended to distinguish the effect of stress diffusion with MSWI layer, to investigate the strain at the underside of the hot mix asphalt (HMA) layer and the stress diffusion through the depth with/without MSWI bottom ash. To verify whether the thickness change of MSWI bottom ash affect the stress and strain is also the propose. The results and figures of different models have been compared and analyzed. The conclusions are as follows:

1. The MSWI layer plays a prominent role of stress diffusion on subgrade layer while there is almost no stress change in the subgrade layer and no displacement change in the subgrade layer.
2. Certain thickness of MSWI layer plays an important role in stress diffusion. However, the increase of layer thickness may result in an unsatisfactory stress distribution in the MSWI bottom ash layer.
3. MSWI layer on the subgrade layer diminishes the tensile strain at the bottom of HMA layer, while MSWI layer on the subgrade layer lessens the compressive strain on top of subgrade layer.
4. It can be concluded from the dynamic loading model of pavement structure that appropriate thickness of MSWI bottom ash layer can decrease the stress and strain through the pavement depth. Based on the finite element simulation results, the recommended thickness of MSWI layer is 10cm. It is indicated that the MSWI layer can alleviate the fatigue and damage due to tire moving load, and MSWI bottom ash is valid as suitable subgrade materials in road construction.

ACKNOWLEDGEMENTS

This study was supported by the National Natural Science Foundation of China (52078317, 51778386, 51708377), Natural Science Foundation of Jiangsu Province (BK20170339), Natural Science Fund for Colleges and Universities in Jiangsu Province (17KJB560008), Open Fund of National Engineering Laboratory of Highway Maintenance Technology (Changsha University of Science & Technology) (kfj180105) and project from Jiangsu Provincial Department of Housing, Urban-Rural Development (2016ZD18 and 2017ZD002).

REFERENCES

1) Aaron, Mwanza., Hao, P.W. and Xiao, M.D. (2013): Evaluation of Permanent Deformation Models in Asphalt Mixture Overlays for Hot Climates, *Advanced Materials Research*.
2) Qadeer, Alam., M.V.A, Florea., K, Schollbach, and H.J.H, Brouwers. (2017): A two-stage treatment for Municipal Solid Waste Incineration (MSWI) bottom ash to remove agglomerated fine particles and leachable contaminants, *Waste Management*. 67: 181-192.
3) Alba, N., Gasso, S., Lacorte, T. and Baldasano, J.M. (1997): Characterization of municipal solid waste incineration residues from facilities with different air pollution control systems, *Journal of the Air & Waste Management Association*, 47: 1170-1179.
4) Arickx, S. T., Gerven, Van., Knaepkens, T., Hindrix, K., Evens, R. and Vandecasteele, C. (2007): Influence of treatment techniques on Cu leaching and different organic fractions in MSWI bottom ash leachate, *Waste Management*, 27: 1422-1427.
5) Bakker, E.J., L, Muchová, P.C. (2007): Rem "Economic recovery of precious metals from MSWI bottom ash,"1st International Conference on Environmental Management, Engineering Planning and Economics (CEMEPE 2007), 1-5.
6) Bayuseno, A.P. and Schmahl, W.W., (2010): Understanding the chemical and mineralogical properties of the inorganic portion of MSWI bottom ash, *Waste Management*, 30: 1509-1520.
7) Bian, X., Cui, Y.J. and Li, X.Z. (2018): Voids effect on the swelling behaviour of compacted bentonite, *Géotechnique*. online, https://doi.org/10.1680/jgeot. 17: 283.
8) Dae-Wook Park. (2007): Simulation of rutting profiles using a viscoplastic model, *KSCE Journal of Civil Engineering*, 11: 151-156.
9) Gajewski, M. and Jemioło, S. (2008): Modelling with FEM test of mineral asphalt mixes resistance to rutting, Theoretical Foundations of Civil Engineering XVI Polish-Ukrainian-Lithuanian Transactions, *Printing House of Warsaw University of Technology*, 131-138.
10) Gao, Y.F., Hang, L., He, J.* and Chu, J. (2019): Mechanical behaviour of biocemented sands at various treatment levels and relative densities, *Acta Geotechnica*, (doi.org/10.1007/s11440-018-0729-3), 14(3): 697-707.
11) Hambleton, J.P. and Drescher, A., (2009): Modeling wheel-induced rutting in soils: Rolling, *Journal of Terramechanics*. 46(2): 35-47.
12) He, J., Gao, Y.F.*, Gu, Z., Chu, J. and Wang, L. (2020): Characterization of crude bacterial urease for CaCO3 precipitation and cementation of silty sand, *Journal of Materials in Civil Engineering*, 32(5): 04020071.
13) Hossam, F.H., Abdelfattah., Khalid., Al-Shamsi., Khalifa. and Al-Jabri. (2016): Evaluation of rutting potential for asphalt concrete mixes containing copper slag, *International Journal of Pavement Engineering*. 630-640.
14) Huang, Y., Guan, Y., Wang, L., Zhou, J., Ge, Z. and Hou, Y. (2017a): "Characterization of mortar fracture based on threepoint bending test and XFEM." *International Journal of Pavement Research and Technology*. DOI: https://doi.org/10.1016/j.ijprt.2017.09.005.
15) Huang, Y., Wang, L. and Xiong, H. (2017b): "Evaluation of pavement response and performance under different scales of APT facilities." *Road Materials and Pavement Design*. 18(S3): 159-169.
16) Huang, Y.C., Chen, J., Shi, S.J., Li, B., Mo, J.L. and Tang, Q. (2020): Mechanical Properties of Municipal Solid Waste Incinerator (MSWI) Bottom Ash as Alternatives of Subgrade Materials, *Advances in Civil Engineering*. DOI: https://doi.org/10.1155/2020/9254516.
17) Luo, Sang., Lu, Qing., Qian, Zhen. Dong., et al. (2017): Laboratory investigation and numerical simulation of the rutting performance of double-layer surfacing structure for steel bridge decks, *Construction and Building Materials*. 144: 178-187.
18) Peng, J.H., Zhang, J.H., Yong, J.L., et al. (2020): Modeling humidity and stress-dependent subgrade soils in flexible pavements, *Computers and Geotechnics*. 120: 103413.
19) Reaz, Imaninasab., Behazad, Bakhshi. and Bahram, Shirini. (2016): Rutting performance of rubberized porous asphalt using Finite Element Method (FEM), *Construction and Building Materials*, 106: 382-391.
20) Salehabadi, E.G. (2012): The Linear Elastic Analysis of Flexible Pavement by the Finite Element Method and Theory of Multiple-Layers System, *Switzerland Research Park Journal*. 101.
21) Shen, J., Wan, L*. and J, Zuo. (2019): Non-linear shear strength model for Coal Rocks, *Rock Mechanics and Rock Engineering*. DOI: 10.1007/s00603-019-01775-y.
22) Tang, Q., Tang, X.W., Li, Z.Z.*, Chen, Y.M., Kou, N.Y. and Sun, Z.F. (2009): Adsorption and desorption behaviour of Pb(II) on a natural kaolin: equilibrium, kinetic and thermodynamic studies, *Journal of Chemical Technology and Biotechnology*, 84: 1371-1380.
23) Tang Q., Katsumi T.*, Inui T. and Li Z.Z. (2014): Membrane behavior of bentonite amended compacted clay, *Soils and Foundations (JGS)*, 54(3), 329-344.
24) Tang, Q., Kim, H.J., Endo, K., Katsumi, T.*, Inui, T., (2015): Size effect on lysimeter test evaluating the properties of construction and demolition waste leachate, *Soils and Foundations (JGS)*, 55(4), 720-736.
25) Tang, Q., Liu, Y., Gu, F.* and Zhou, T. (2016a): Solidification/stabilization of fly ash from a municipal solid waste incineration facility using Portland cement, *Advances in Materials Science and Engineering*, vol. 2016, Article ID 7101243, 10 pages, 2016. doi:10.1155/2016/7101243.
26) Tang, Q., Wang, H.Y.*, Tang, X.W. and Wang, Y. (2016b): Removal of aqueous Ni(II) with carbonized leaf powder: kinetic and equilibrium studies, *Journal of Central South University*, 23: 778-786.
27) Tang, Q., Zhang, Y., Gao, Y.F. * and Gu, F. (2017): Use of Cement-Chelated Solidified MSWI Fly Ash for Pavement Material: Mechanical and Environmental Evaluations, *Canadian Geotechnical Journal*, 54(11): 1553-1566.
28) Tang, Q., Gu, F.*, Zhang, Y., Zhang, Y.Q. and Mo, J.L. (2018a): Impact of biological clogging on the barrier performance of landfill liners, *Journal of Environmental Management*, 222: 44-53.
29) Tang, Q., Gu, F.*, Chen, H., Lu, C. and Zhang, Y. (2018b): Mechanical Evaluation of Bottom Ash from Municipal Solid Waste Incineration Used in Roadbase, *Advances in Civil Engineering*, Volume 2018, Article ID 5694908, https://doi.org/10.1155/2018/5694908.
30) Tang, Q., Shi, P.X.*, Yuan, Z., Shi, S.J., Xu, X.J. and Katsumi, T.* (2019a): Potential of zero-valent iron in remediation of Cd(II) contaminated soil: from laboratory experiment, mechanism study to field application, *Soils and Foundations (JGS)*, 2019.11.005, 59: 2099-2109.
31) Tang, Q., Shi, P.X.*, Zhang, Y., Liu, W. and Chen, L. (2019b): Strength and Deformation Properties of Fiber and Cement Reinforced Heavy Metal-Contaminated Synthetic Soils, *Advances in Materials Science and Engineering*, Volume 2019, Article ID 5746315, 9 pages, https://doi.org/10.1155/2019/5746315.
32) Vegas, I., Ibañez, J.A., San, José, J.T. and Urzelai, A. (2008):

Construction demolition wastes, Waelz slag and MSWI bottom ash: A comparative technical analysis as material for road construction, *Waste Management*. 28: 565-574.

33) Wang, Yuke., Gao, Yufeng., Guo, Lin. and Yang, Zhongxuan. (2018): Influence of intermediate principal stress coefficient and principal stress direction on drained behavior of natural soft clay, *ASCE International Journal of Geomechanics*. 18(1), 04017128.
34) Wen, K.H., Xiao, N.Z., Hong, L.R. and Bo, C. (2015): Finite element method for predicting rutting depth of steel deck asphalt pavement based on Accelerated Pavement Test. In: 3rd International Conference on Mechanical Engineering and Intelligent Systems, 935-942.
35) Zeng, Ling., Xiao, Liuyi., Zhang, Junhui. and Gao, Qianfeng. (2019): Effect of the characteristics of surface cracks on the transient saturated zones in colluvial soil slopes during rainfall, *Bulletin of Engineering Geology and the Environment*, Doi: 10.1007/s10064-019-01584-1.
36) Zhang, Junhui., Peng, Junhui., Liu, Weizheng. and Lu, Weihua. (2019a): Predicting resilient modulus of fine-grained subgrade soils considering relative compaction and matric suction, *Road Materials and Pavement Design*, Doi: 10.1080/14680629.2019.1651756.
37) Zhang, Junhui., Peng, Junhui., Zeng, Ling., Li, Jue. and Li, Feng., (2019b): Rapid Estimation of Resilient Modulus of Subgrade Soils Using Performance-Related Soil Properties, *International Journal of Pavement Engineering*, Doi: 10.1080/10298436.2019.1643022.
38) Zhang, Junhui., Gu, Fan. and Zhang, Yuqing. (2019c): Use of building-related construction and demolition wastes in highway embankment: Laboratory and field evaluations, *Journal of Cleaner Production*, 230: 1051-1060. Doi: 10.1016/j.jclepro.2019.05.182.
39) Zhang, J.P., Zhu, C.Z., Li, X.Q., Pei, J.Z. and Chen, J. (2017): Characterizing the three-stage rutting behavior of asphalt pavement with semi-rigid base by using UMAT in ABAQUS. *Construction and Building Materials*, 140: 496-507.
40) Zhang, Y., Tang, Q*., Chen, S., Gu, F. and Li, Z.Z. (2018): Heavy metal adsorption of a novel membrane material derived from senescent leaves: kinetics, equilibrium and thermodynamic studies, *Membrane Water Treatment*, 9(2), 95-104.